

# The Radio-Loud Plasma in Pulsars

J. A. Eilek<sup>1</sup>, P. N. Arendt, Jr.<sup>1</sup>, T. H. Hankins<sup>1</sup> and J. C. Weatherall<sup>1</sup>

New Mexico Tech, Socorro NM 87801, USA

**Abstract.** The pulsar magnetosphere contains a strongly magnetized, relativistic plasma. We need to understand the physics of that plasma if we want to connect the data to the models. Our group in Socorro is mixing theory and observations in order to study the radio-loud pulsar plasma. In this paper we report on several aspects of our current work.

## 1. Introduction

We know pulsars produce radio emission at high brightness temperatures. It is very likely that this arises in a plasma. We also know that high- $T_B$  emission is created by dynamical, non-equilibrium plasma processes elsewhere in space or astrophysical plasmas. Therefore, we can safely guess that the process by which pulsars shine involves a plasma. This is, however, not saying much. We know very little about the origin or dynamics of the radio-loud plasma. This is unfortunate, because understanding the pulsar plasma is critical to understanding the star. The radiation from that plasma is the only data we can get from these interesting stars. If we want to connect the observations to the physics (including the wealth of new, high-quality data becoming available, such as presented at this meeting), we need to study the plasma.

This paper is organized around two questions. What do we know about the radio-loud plasma in the pulsar? Can insight and methods from other areas of plasma astrophysics be applied here? More specifically, can we understand the dynamical state of the plasma (which connects back to the electrodynamics of the system), and how it produces the observed radiation (which is a consequence of its dynamical state)?

We begin with an overview (§2-5) of standard pulsar theory and what that theory requires, or suggests, about the plasma. One common assumption is that the radio emission comes from a lepton pair plasma. In §6-7 we report on work carried out by two of us (Arendt & Eilek) which follows the pair cascade numerically and determines the details of the lepton plasma produced by the cascade. After that, in §8-9 we suggest that time variability might

be the best observational diagnostic of the plasma, and we report on ongoing work by two of us (Weatherall, Eilek) to model the plasma dynamics on short timescales. We close with a report (§10) on ultra-high time resolution observations of the Crab pulsar carried out by one of us (Hankins) which we believe begin to address some basic theoretical issues regarding plasma dynamics and the emission mechanism.

## 2. The standard model and its Limitations

To set the stage, we review the standard model, with an eye to its consequences for plasma formation and dynamics. This model has been carefully developed by many people over the years, and has had good success. But it also has its limitations; now that we have a common theoretical ground, and now that we have some excellent new data (including single-pulse work, polarimetry, multifrequency studies and millisecond pulsar studies), it is time to review the model with a critical eye. The areas where it fails will be the areas which can be fruitfully revisited. In this paper we limit ourselves to the radio emission region, and leave high-altitude, high-energy issues to others.

### 2.1. A corotating magnetosphere

A strong magnetic field is tied to a rapidly rotating neutron star. It contains and structures a plasma-filled magnetosphere. Most of the field lines which leave the star's surface reverse direction within the light cylinder and return to the star (as illustrated in Figure 1). It is natural to consider a steady atmosphere in this region, *i.e.*, one which rotates with the star. This can be maintained if an electric field exists,  $\mathbf{E}_{co}$ , which satisfies

$$\mathbf{E}_{co} + \frac{1}{c}(\boldsymbol{\Omega} \times \mathbf{r}) \times \mathbf{B} = 0 \quad (1)$$

Such a field produces an  $\mathbf{E}_{co} \times \mathbf{B}$  drift equal to the corotation speed. This field must be supported by a nonzero charge density,

$$\rho_{GJ} = \frac{1}{4\pi} \nabla \cdot \mathbf{E}_{co} \simeq -\frac{\boldsymbol{\Omega} \cdot \mathbf{B}}{2\pi c} \quad (2)$$

This is called the “corotation” or “GJ” density. Note that the plasma must be non-neutral in order to corotate; most of the magnetosphere is usually assumed to contain a single sign of charge.

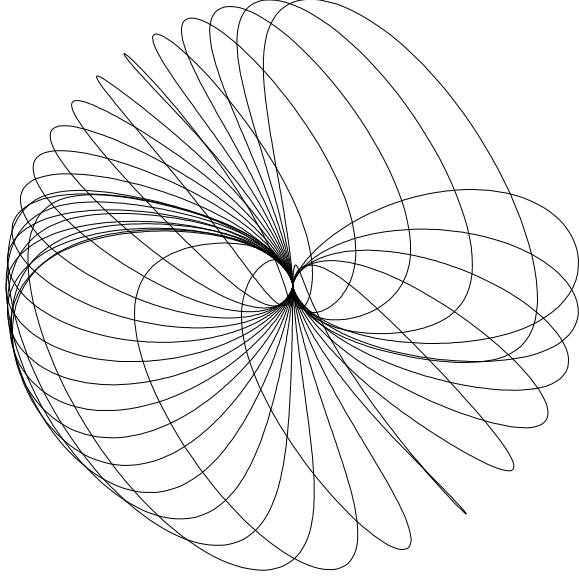


**Fig. 1.** The magnetosphere of a pulsar, illustrated by the last open field lines in a rotating vacuum magnetic dipole, at an  $45^\circ$  inclination angle to the rotation axis, viewed looking down the rotation axis. Relativistic effects distort the field lines close to the light cylinder. Most of the magnetosphere, within the closed field lines, is assumed to corotate with the star. The open field line region (or polar flux tube, PFT) allows a current-carrying outflow from the star, is thought to contain a dense electron-positron plasma, and to be the origin of the radio emission. Despite the high-altitude field distortions due to relativity, the PFT is nearly circular in cross section at radio emission altitudes. From Arendt (2002).

### 2.2. The acceleration region

Conditions are different in the polar flux tube (PFT). This is the narrow region defined by field lines which do not close within the light cylinder. In this region, relativistic outflow from star’s surface is thought to occur, driven by deviations from the corotation density. These deviations can support an  $\mathbf{E}$  field with a non-zero component parallel to the  $\mathbf{B}$  field;  $\mathbf{E}_{\parallel}$  can accelerate particles to high energies.

The standard model now has a branch point, with two specific but different variants proposed (*e.g.*, Ruderman & Sutherland 1975, Arons & Scharleman 1979). One variant assumes that charges cannot freely leave the star’s surface, and thus a “vacuum gap” exists just above the

surface. Strong  $\mathbf{E}_{\parallel}$  in this gap accelerates particles to relativistic energies, perhaps in a non-steady fashion (sparking, breakdown). Another variant assumes that charges can freely leave the star’s surface. If the charge density deviates from corotation,  $\mathbf{E}_{\parallel}$  created by these charges will enable their acceleration, also to relativistic energies.

This low-altitude acceleration creates a highly relativistic “primary beam”, which gains significant fraction of the maximum potential drop in a short distance. Most authors assume the acceleration region is limited by pair formation, which is believed to shield  $\mathbf{E}_{\parallel}$ . Alternatively, the acceleration may be limited by radiative losses before the energies required for pair formation are reached (Sturmer 1995; Jessner *et al.* 2001).

### 2.3. The Pair Cascade

A very important step is taken here. Radiation from the primary beam charges is assumed to seed a  $\gamma B$  pair cascade. Either curvature radiation (if the charges reach  $\gamma \sim 10^7$ ) or magnetic-resonant Compton scattering (if they reach  $\gamma \sim 10^4$  and the star is a thermal X-ray source) produces energetic photons. These photons, in the star’s strong  $B$  field, can produce an electron-positron pair. Further photon production by these daughter leptons leads to further pair production, thus initiating a cascade of particle creation. The end point of this cascade is often assumed to be total conversion of the primary beam energy to much slower (but still relativistic) leptons, with very high multiplicities ( $\mathcal{M}$ , defined as the number of daughter leptons per primary beam particle).

Two additional important assumptions follow; neither of them has been clearly established to be true. One is that the pair plasma terminates the acceleration region, by shielding the accelerating  $E$  field. The second is that the pair plasma is the means by which the free energy available in the primary beam is converted to coherent radio emission. We discuss both in more detail later.

## 3. Annoying Issues and Inconsistencies

Some problems remain in this picture.

### 3.1. The Density is a Problem

We do not know the details of the radio emission mechanism, but the local plasma frequency,  $\nu_p$ , is likely to be important. Plasma turbulent models predict emission at close to  $\nu_p$ . Signal propagation is suppressed below  $\nu_p$  (except at angles very close to  $\mathbf{B}$ ). However, the numbers do not work. (Others have also noticed this problem: *cf.* Kunzl *et al.* 1998, or Melrose 2000).

Consider a plasma of number density  $n$ , moving at bulk Lorentz factor  $\gamma$ . It supports plasma waves with frequency  $\nu_p^2 = \gamma n e^2 / \pi m$  (all quantities measured in the star’s frame). The standard model predicts the number density

is at least that required by corotation,  $n_{\text{GJ}} = \rho_{\text{GJ}}/e$ ; pair creation amplifies this by the multiplicity  $\mathcal{M}$ . If we use (2) and scale to the field at the stellar surface, this predicts a plasma frequency

$$\nu_{\text{p}} = \left( \frac{\gamma e B \mathcal{M}}{4\pi m c P} \right)^{1/2} \simeq 1.2 \left[ \frac{\gamma B_{*,12} \mathcal{M}}{P(r/r_*)^3} \right]^{1/2} \text{ GHz} \quad (3)$$

Now,  $\gamma \mathcal{M} \gg 1$  in most models, and  $r \sim 3-30r_*$  is the typical range of emission altitudes. Thus, the standard model predicts  $\nu_{\text{p}} > 1$  GHz, and we should see little radiation at lower frequencies. On the other hand, pulsars are strong radio sources down to frequencies  $\sim 10$  MHz. We consider this a problem.

To resolve this problem, either the radiation must emerge well below the plasma frequency, or the plasma density in at least part of the radio-loud region is much lower than commonly thought. We think the latter case is more likely. It must follow that steady corotation is not obeyed; the plasma will be dynamically variable.

### 3.2. The Plasma is not Steady

We note two further hints of an unsteady plasma.

No pulsar has steady radio emission. We see modulation on all time scales where we've looked, from sub- $\mu\text{s}$  flickering to mode changes and nulls on multi-period timescales. Coherent radio emission is a very nonlinear-gain process, so we expect small fluctuations in the plasma to be strongly amplified. Nonetheless, this observed variability tells us that the plasma flow cannot be as steady as in most of the models. As with the density problem, this suggests to us that the plasma does not satisfy corotation. Density deviations lead to a net force in the corotating frame, and these forces should lead to nonsteady flows.

Furthermore, the assumption of a steady, corotating magnetosphere with no flows is only self-consistent for an aligned rotator. We note two interesting features of a star whose magnetic axis is not aligned with its rotation axis. (1) The  $\mathbf{E} \times \mathbf{B}$  drift velocity has a component along  $\mathbf{B}$ . Unless the plasma is charge-neutral (recall  $\rho_{\text{GJ}}$  carries a sign), this will drive field-aligned currents even in corotating regions. (2) The ‘‘GJ current’’,  $j_{\text{GJ}} \propto \rho_{\text{GJ}}$ , has a non-zero divergence. Non-steady flows are therefore required by charge conservation, unless the magnetosphere is fully static (which is highly unlikely). Both of these effects may be small, but they also hint at non-steady plasma flows in the magnetosphere.

### 3.3. Where is the acceleration region?

The standard model predicts a very low-altitude acceleration and pair cascade region. On the other hand, the radio-loud region is thought to be at least several stellar radii above the surface. The emission altitude is determined from the data through a quasi-universal set of assumptions: that the radio emission arises only in the PFT,

that the magnetic field is dipolar, and that the mean profile width is due to the star rotating past one's sightline. Details of the deprojection vary between authors (*e.g.*, Rankin 1993, Kijak & Gil 1998, or Eilek & Hankins 2002), but there is general agreement that the emission altitude lies between a few and a few tens of stellar radii.

We find this unsatisfying. Once the pair plasma is formed it should radiate almost immediately. The plasma turbulence thought to lead to radio emission should develop quickly. Thus, if the acceleration and pair formation region is indeed close to the star, the radiation must remain confined in the PFT plasma until it escapes at a few tens of stellar radii. Plasma trapping of the radiation, when the wave frequency is below the local plasma frequency, has of course been assumed to explain this. However, we now know that the density distribution of the PFT is not as simple as was once thought. We also note that radiation wavevectors at small angles to  $\mathbf{B}$  can propagate below the local plasma frequency. The entire situation would be simpler if the radio emission region were also the acceleration and pair formation region (*e.g.*, Shibata 1991).

### 3.4. Do all pulsars have a pair cascade?

The pair cascade is an important part of the standard model. Its onset is determined by the acceleration rate in the ‘‘gap’’ region. The dense plasma it produces is assumed to shield the accelerating  $\mathbf{E}$  field, and thus end the gap. But this cartoon is not self-consistent. When the standard model is made quantitative, one finds that the pair cascade is unlikely to occur in pulsars with magnetic field  $\lesssim 10^{11}$  G (Arendt & Eilek 2002; details below). This means that neither old, isolated pulsars, nor msec pulsars, should show pair formation, if they obey the standard model.

How can this be resolved? Either (i) not all pulsars have a dense pair atmosphere (and thus are ‘‘pairless’’ radiators), or (ii) our standard model is seriously lacking; or perhaps (iii) both of the above are true.

### 3.5. Is Magnetic Field Dipolar?

The assumption that the magnetic field is dipolar lies at the heart of the standard model. Detailed development of that model usually assumes a purely dipolar field. There are various hints, however, that this is not the full picture. Some authors have suggested that the low-altitude field is more complicated – a stronger field with more complex structure near the surface may help the problem of pair formation in weak-field pulsars. Such ideas may well be supported by the data. There has been some very good work on polarization in recent years (*e.g.*, van Hoensbroeck & Xilouris 1997, or Hankins & Rankin 2002). We now know (*e.g.*, Eilek & Hankins 2000) that the linear polarization in an interesting subset of bright pulsars is *not* well explained by the usual rotating-vector model. Thus,

the field is very likely to deviate from dipolar, *even in the radio emission region*.

#### 4. Larger Unsolved Questions

The standard picture contains (at least) two major, unsolved questions. These are not new questions, and work continues on each – with no consensus as to the answer.

##### 4.1. The Pulsar Circuit

An outflow of relativistic charged particles, along open field lines, is a fundamental part of the pulsar model. This constitutes a current. The nature of the pulsar circuit is still far from understood: where does the current return to the star? Is the circuit open (to the ISM) or closed? How is the current driven (that is, how does the rotational potential of the star couple to the current flow?) The literature contains two approaches to this problem. Models of the low-altitude acceleration region (possibly with pair formation) describe in detail the dynamics of individual charges in that region. This region is assumed also to drive the current. If the outflowing plasma is relativistic, fills the PFT, and is at the corotation density, then the magnitude of the current follows directly:  $I = \rho_{\text{GJ}} c A_{\text{PFT}}$ . These models rarely address the rest of the circuit.

An alternative approach is to consider the global circuit. The dynamo must still be the star's rotation, which creates a potential drop in any plasma which is not corotating with the star.<sup>1</sup> This approach allows the possibility of localized resistive regions (“loads”; possibly the inner or outer gaps) where energy is dumped into plasma, then radiation (*e.g.*, Kunzl *et al.* 2002). In principle, the combination of the driving voltage and the resistance of the circuit will determine the magnitude of the current. We see no *a priori* reason for this to be the GJ current (Shibata, 1991, has made this point nicely).

These models have not yet been developed at the level of the low-altitude acceleration region models, but we find them attractive. One might hope that observational diagnostics could be developed (of such quantities as current density or circuit length). We return to this issue in §8-9.

##### 4.2. The Radiation Mechanism

How does the pulsar shine? We do not have a simple model of how the plasma produces the very high brightness temperatures characteristic of the radio emission. Most authors believe either the primary beam or the pair plasma will be susceptible to plasma instabilities (such as beam bunching or the two-stream instability). Some of these in-

stabilities will grow to nonlinearity and couple to electromagnetic radiation which can escape the system.

Within this general picture much variety is possible. Models abound, and some have been developed in great detail, but with no consensus as to which is the most relevant to real pulsars, and with hardly any useful observational discriminants proposed. (For instance, *cf.* Melrose 1992, or Lyubarski, this meeting). We might group the models currently being discussed into three categories. One starts with *coherent charge bunches*. Early emission models assumed that such bunches produced curvature emission in the radio range. An interesting recent variant is Compton scattering of plasma emission by such bunches (*e.g.*, Kunzl *et al.* 2002). A second class of models invoke strong *plasma turbulence*, in which soliton growth and possible collapse convert plasma wave energy into escaping radiation (*e.g.*, Asseo *et al.* 1990, Weatherall 1997). A third type of model uses *maser-like* mechanisms, which convert internal energy of the plasma to radio emission (*e.g.*, Luo & Melrose 1995, Kazbegi *et al.* 1991, Weatherall 2001).

All of these models differ in their details, and often in their deductions about the significant properties of the emission (such as its spectrum, spatial location, or relation to local plasma conditions). One might also hope that observational tests of the models could be developed. We also return to this question in §8-9, below.

#### 5. The State of the Radio-Loud Plasma

To return to our original question: what do we know, or assume, about the plasma in the radio-loud region?

*Composition.* The plasma is probably dominated by electron-positron pairs in the radio-loud region (although this is not established for slow and msec pulsars). It is also not charge neutral (in order to maintain corotation).

*Number density.* The plasma is assumed either to be at the corotation density,  $n_{\text{GJ}} = \rho_{\text{GJ}}/e$ , or to be increased over this by the pair multiplicity  $\mathcal{M}$ . Both of these assumptions are common in the literature; as we point out above, both assumptions are inconsistent with observed low-frequency radio emission. We suspect (in agreement with Melrose 2000) that the plasma is highly inhomogeneous, with radio emission coming from the lower-density regions, and the corotation density possibly being met in some average fashion.

*Plasma “beta”.* The plasma is highly magnetized, with  $B \sim 10^{11} - 10^{13}$  G at the surface of single pulsars. It is therefore strongly field dominated; the inertia and energy density of the plasma are tiny compared to the magnetic field.

<sup>1</sup> This may be the magnetosphere, which some authors assume rotates at a slightly different rate from the star itself, or could be the ambient ISM, which is magnetically connected to the star *via* the open field lines.

*Flows.* The plasma flow is highly relativistic and one-dimensional:  $\gamma \sim 100 - 10^7$  (depending on author). The flow is nearly along the magnetic field, with slow cross-field drifts in regions where transverse  $\mathbf{E}$  fields exist. The gyromotion of individual charges is quantized, with most particles in the lowest Landau levels.

*Dynamical state.* The plasma is very likely to be inhomogeneous and unsteady. We know collective effects are needed to produce coherent radio emission. Thus the plasma is likely to be strongly turbulent on microscales. We also infer a nonsteady state from the nonsteady radio emission. Finally, if the plasma contains low-density regions, we expect the unshielded electric field to keep the plasma dynamically active.

*Plasma distribution function.* This important part of any plasma physics study has remained unconstrained until recently. Previous authors have either assumed analytically convenient forms, or tried to quantify semi-heuristic arguments. New work, on which we report below, shows that the pair plasma is well described by a relativistic Maxwellian, at  $k_B T \sim mc^2$ , in the comoving frame.

## 6. The Cascade and the Plasma it Produces

We now turn to the pair cascade: when and how does it occur, and what is the nature of the plasma it produces? The cascade begins with a seed photon, of energy  $\epsilon = h\nu/mc^2$ , which pair creates *via*  $\gamma + B \rightarrow e^+ + e^- + B$ . The newly created leptons will emit synchrotron radiation if they are created in upper Landau levels. If this is the case the synchrotron photons will themselves pair create, thus extending the cascade to several generations.

This is an inherently nonlinear process, not well suited to analytic methods (although progress can be made with heroic effort, *e.g.*, Hirschman & Arons 2001). Numerical simulation are called for. Daugherty and Harding (1982) led the way with simulations which determined the spectrum of hard photons escaping from a cascade region. We revisited the subject in order to learn more about the pair plasma. Our goal was to simulate a cascade produced according to the standard models. That is, we did not attempt a self-consistent treatment of the plasma electrodynamics within the acceleration region. Rather, we assumed the primary beam particles had energies typical of what is found in the literature, and they produce seed energetic photons either by curvature radiation (CR) or inverse Compton scattering (ICS). We summarize our results here; more details can be found in Arendt (2002), and Arendt & Eilek (2002).

### 6.1. Details of the calculation

Our calculations were based on monoenergetic photon “kernels”. For each of these, we started with photons of a fixed energy, moving at a small range of angles (such as given by relativistic beaming) relative to the local  $\mathbf{B}$ . We followed each in time and space (assuming linear propagation relative to a non-rotating frame, ignoring general relativistic effects) until it had a unit opacity to pair creation. At that point the differential cross section and Monte Carlo methods were used to create daughter leptons. We followed each lepton in time and space (assuming guiding-center motion along  $\mathbf{B}$ , ignoring acceleration by any local  $\mathbf{E}_{\parallel}$ ) until it had unit opacity to synchrotron radiation. At that point Monte Carlo methods were again used to create new photons. This process continued, following all quanta in time and space, until all the action had stopped—that is until no further pair or photon creation occurred. The end of such a calculation gave us one “kernel”.

We convolved the kernels with the seed photon distributions produced by CR or ICS to determine the plasma and photon distributions predicted by cascades in a pulsar. We chose primary beam energies  $\gamma_p \sim 10^6 - 10^7$  for cascades seeded by CR, and  $\gamma_p \sim 10^3 - 10^5$  for cascades seeded by magnetic-resonant ICS. We simulated full cascades for magnetic fields  $B = 10^{12}\text{G}$  and  $10^{13}\text{G}$ . We also explored cascades in  $B = 10^{11}\text{G}$  fields, but found they were very expensive in computer time, due the large numbers of soft photons created for each lepton pair produced. Thus we only included the two larger field strengths in our final results.

### 6.2. Onset of the Cascade

The cascade can be understood in terms of the two governing principles, energetics and opacity. Recall that an electron at energy  $\gamma_p$  produces a curvature radiation spectrum which peaks at a photon energy  $\epsilon_{\text{CR}} = \hbar\omega_{\text{CR}}/mc^2 \sim 3ch\gamma^3/2\rho mc$ , where  $\rho$  is the radius of curvature of the field line. Magnetic resonant ICS produces photons in the range  $\epsilon_B/2\gamma_p \leq \epsilon \leq 2\gamma_p\epsilon_B$ , where  $\epsilon_B = \hbar\omega_B/mc^2 = B/B_c$ .

Consider a seed photon, of energy  $\epsilon$ , moving at an angle  $\theta$  relative to  $\mathbf{B}$ . Two conditions must be satisfied if it is to pair produce. The first condition is energetics. The available photon energy must satisfy  $\epsilon > 2mc^2$ . Relativistic kinematics expands this as

$$\epsilon_{\perp} = \epsilon \sin \theta > 2. \quad (4)$$

(in the star’s frame). We found that most of the pair creation in our high-field runs was governed by energetics. Photons travelling nearly parallel to  $\mathbf{B}$  propagate freely until field line curvature finally establishes  $\epsilon_{\perp} > 2$ . Pair creation then proceeds immediately. Most of the newly created leptons are in the ground Landau state, so they cannot create further photons, and the cascade ends.

The second condition that must be met for pair creation is opacity. The photon must have a significant chance of creating a pair. Using the basic cross section, one can show that this requires

$$\epsilon B \gtrsim 0.1 B_c \sim 4 \times 10^{12} \text{G} \quad (5)$$

again in the star's frame (this is the best case, that of  $\theta = \pi/2$ , a right angle crossing of the magnetic field line). We found that our lower field runs, and some initial creation events in our high field runs, were opacity dominated. The parent photons have more than enough energy to produce a pair, but the probability of pair production is low until they propagate to an angle such that  $\epsilon_{\perp} \lesssim 0.1 B_c/B$ . The newly created leptons in this case tend to be born in excited Landau levels. They then decay *via* the production of energetic synchrotron photons, which extend the cascade to several further generations.

These two conditions make it clear that the magnetic pair cascade does not necessarily occur in all pulsars. In particular, stars with a weak  $B$  field need very energetic photons to satisfy the opacity condition; such high energies are not produced by the two standard seed-photon radiation models (*e.g.*, Weatherall & Eilek 1997). It is traditional to invoke highly curved fields in old and millisecond pulsars, assuming that this will enable pair production. We caution, however, that the acceleration of the primary beam charges, and the spectrum of their radiation, must be shown to work quantitatively before the pair cascade can be demonstrated to occur in all pulsars.

### 6.3. Development and Decay of the Cascade

We found, as expected, that pair formation is enhanced towards the edge of the PFT, due to the larger field line curvature there. We would thus expect “conal” emission from the pair plasma; as others have pointed out, “core” emission does not easily fit into this picture.

We continued our simulations until all reactions had stopped – until there were no remaining photons with energy and opacity to create further pairs. In all cases the cascade ended before the quanta reached one stellar radius from their injection point. Thus, the pair cascade is a rapid process, with the time from seed photon emission to cascade completion being less than  $R_*/c \sim 30 \mu\text{s}$ . If the seed photon production is sporadic, the pair plasma should be highly nonuniform within the PFT.

### 6.4. Efficiency and Multiplicity of the Cascade

The fraction of the primary beam energy converted into the pair plasma, and the abundance of that plasma, are key parameters in many models of the pulsar magnetosphere and its interaction with the ambient ISM. *Our numerical results do not support assumptions commonly made in the literature.*

**Table 1.** Summary of results from cascade simulations

Curvature Radiation:			
$B = 10^{12} \text{G}:$		$B = 10^{13} \text{G}:$	
$\gamma_p \sim 5 - 10 \times 10^6$		$\gamma_p \sim 2 - 10 \times 10^6$	
$\mathcal{M} \sim 300 - 1000$		$\mathcal{M} \sim 500 - 2000$	
$f_{e^+e^-} \sim 0.03 - 0.1$		$f_{e^+e^-} \sim 0.4 - 0.5$	
$\gamma_{\text{CM}} \sim 80 - 480$		$\gamma_{\text{CM}} \sim 60 - 600$	
$f_{\nu} \sim 0.02 - 1.0$		$f_{\nu} \sim 0.001 - 0.03$	
Inverse Compton:			
$B = 10^{12} \text{G}:$		$B = 10^{13} \text{G}:$	
$\gamma_p \sim 2 - 50 \times 10^4$		$\gamma_p \sim 2 - 10 \times 10^4$	
$\mathcal{M} \sim 10 - 100$		$\mathcal{M} \sim 2 - 10$	
$f_{e^+e^-} \sim 0.1 - 0.3$		$f_{e^+e^-} \sim 0.8 - 1.0$	
$\gamma_{\text{CM}} \sim 60 - 400$		$\gamma_{\text{CM}} \sim 100 - 900$	
$f_{\nu} \sim 0.1 - 0.8$		$f_{\nu} < 0.01$	

$\gamma_p$  is the energy of the primary beam charges.  
 $\mathcal{M}$  is the multiplicity: the number of pairs per primary charge.  
 $f_{e^+e^-}$  is the energy efficiency: the fraction of the primary beam energy that goes into leptons.  
 $\gamma_{\text{CM}}$  is the center of momentum energy of the created leptons.  
 $f_{\nu}$  is the photon energy efficiency: the fraction of the primary beam energy that goes into photons.  
 Full details can be found in Arendt & Eilek (2002), or Arendt (2002).

One common assumption is that the entire energy of the primary beam is transferred to the plasma. We found this is not always the case. Instead, much of the beam energy escapes as photons. The fraction of beam energy going into the pairs ranges from  $f_{e^+e^-} \lesssim 1.0$  in higher magnetic fields, to  $f_{e^+e^-} \lesssim 0.1$  in lower magnetic fields. Another common assumption is that the multiplicity (the number of pairs produced per primary beam particle) is high; a value  $\mathcal{M} \sim 10^4$  is often found in the literature. We found much lower values. The high-field runs, with Compton seeds, were strongly limited by energetics and produced only a few pairs per primary charge. Multiplicities for the lower field and curvature-seed runs ranged from  $O(10)$  to  $O(1000)$ , and increased strongly with primary beam energy. Table 1 summarizes the range of  $f_{e^+e^-}$  and  $\mathcal{M}$  found in our runs; more details can be found in the original papers.

### 6.5. Lepton Distribution from the Cascade

One of our primary goals in these simulations was to determine the momentum distribution function (DF) of the pair plasma created by the cascade. We found a very simple result. Despite the wide range in cascade parameters and pair creation efficiencies encountered, the final DF's have remarkably similar shapes. Figure 2 shows some examples of DF's seeded by both CR and by ICS, *as viewed in the star's frame*. The DF's are all broadly similar, with

a strong peak at moderate energies and an extended high-energy tail. There are slight differences due to the magnetic field. In the  $B = 10^{13}\text{G}$  runs, there are no slow leptons; all DF's have a low- $p_{\parallel}$  gap below  $\sim 20mc$ . In contrast, all of the  $B = 10^{12}\text{G}$  runs have leptons down to  $p_{\parallel} < .01mc$ . (This difference is due to the importance of synchrotron losses, and the energy degrading of multiple lepton generations, in the lower-field runs).

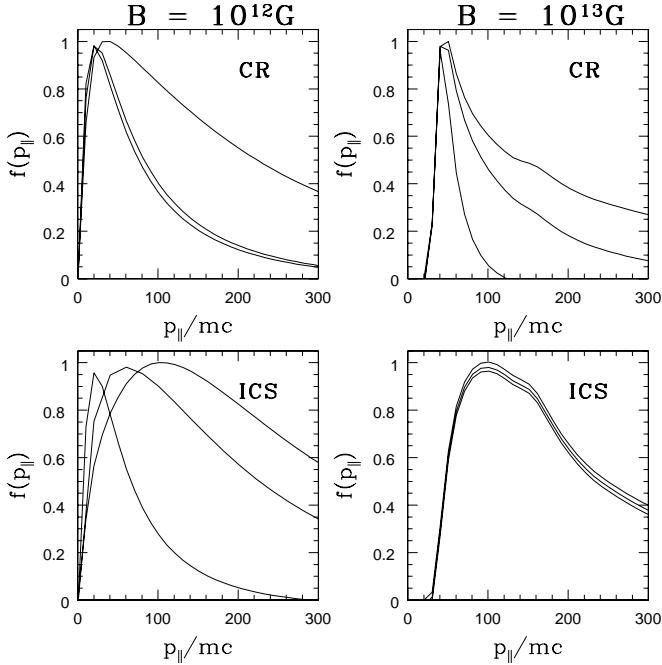


**Fig. 2.** The one-dimensional momentum distribution function of the pair plasma created in the cascade, *as viewed in the star's frame*. The results are shown for two magnetic fields, for cascades seeded by CR with  $\gamma_p = 1, 2, 5 \times 10^6$ , and by ICS with  $\gamma_p = 2, 5, 10 \times 10^4$ . From Arendt & Eilek (2002).

The numerical results simplify nicely if the DF's are transformed to the center-of-momentum (CM) frame of the plasma. (We found that  $\gamma_{\text{CM}} \sim 10 - 100$  over the set of runs). Figure 3 shows the same DF's as in Figure 2, but seen in the CM frame. In this frame, the DF's are remarkably close to a *thermal* distribution, *i.e.* a relativistic Maxwellian:

$$f(p_{\parallel}) \propto \exp[-\zeta\gamma(p_{\parallel})] \quad (6)$$

The parameter  $\zeta$  can be identified with the inverse temperature of the plasma. We carried out numerical fits of this expression to our CM-frame DF's, and found that  $k_B T/mc^2 \sim 0.8 - 2$  describes the full range of our results.

Thus, the DF of the cascade-produced pair plasma is remarkably simple. It is a warm ( $k_B T \sim mc^2$ ) relativistic Maxwellian when viewed in a frame moving with the

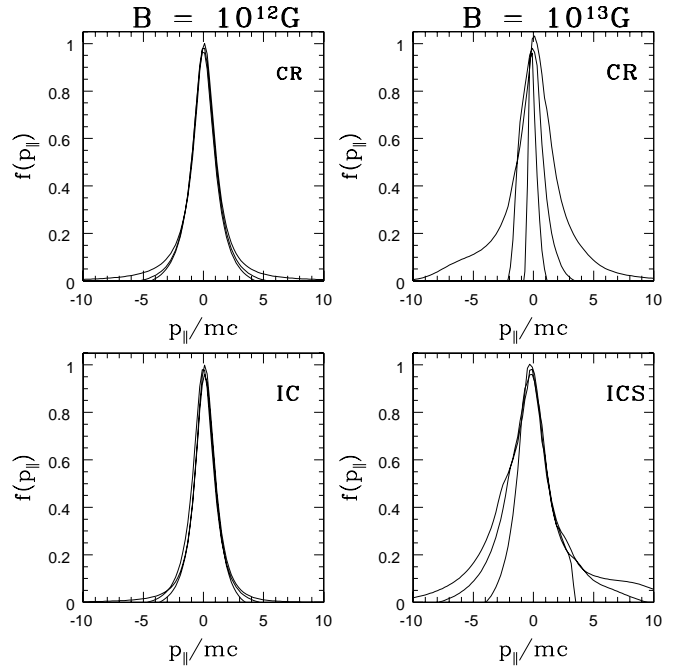


**Fig. 3.** The one-dimensional momentum DF of the pair plasma created in the cascade, *as viewed in the comoving frame*. See Figure 2 for details. From Arendt & Eilek (2002).

plasma. The distorted shape as seen in the lab is simply due to the Lorentz boost when passing to that frame.

### 6.6. Photon Distribution from the Cascade

We also determined the spectrum of the energetic photons which remained after the end of the cascade. This is a composite of secondary photons, produced by synchrotron emission of the pairs, and seed photons which never pair produced.<sup>2</sup> Figure 4 shows a selection of these spectra, presented as number counts (not energy spectra). The photon spectra tended to be steeper in lower magnetic fields, due to secondary synchrotron emission being more important in those cascades. Conversely, the spectra are flatter in the high field runs, where synchrotron photons are rare and the photon spectra are dominated by the seed photons which escaped pair creation. All spectra show a high-energy turnover which comes from the input seed photon distribution.

The fraction of the primary beam power that remained in the photons,  $f_{\nu}$ , was quite low for the high-field runs, especially those with ICS seed; nearly all of the beam energy did go into leptons in those cases. The lower-field runs ended with a large fraction of the beam energy in

<sup>2</sup> Some photons never satisfied the opacity and energy criteria. We distributed the seed photons over angle, within a small range identified with  $1/\gamma_p$ ; those at lower angles had a good chance of escaping the region without pair producing.

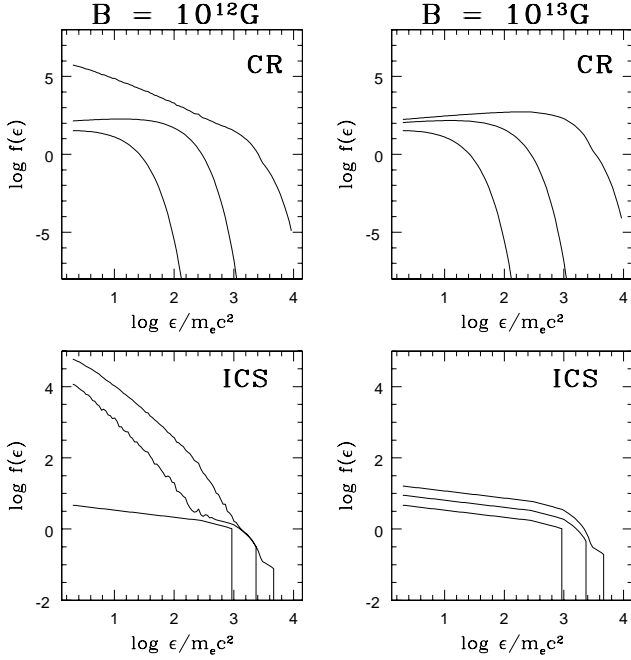


**Fig. 4.** The photon number counts (not the energy spectrum) resulting from the pair cascade, in the star’s frame. See Figure 2 for details. From Arendt & Eilek (2002).

photons:  $f_\nu \sim 0.1 - 1$  in those runs. The large numbers of photons produced in our exploratory runs at  $B = 10^{11} \text{G}$  suggest  $f_\nu$  would be quite large there as well.

## 7. Why does the DF matter?

The reader who is not a plasma theorist may wonder at our emphasis on the plasma DF. Our answer is that it is crucial to understanding the emission and propagation of the radio signal, and that it may have important consequences for the electrodynamics of the emission region.

### 7.1. Coherent Radio Emission

As we noted above, the means by which pulsars produce coherent radio emission are still unknown. There is a general sense that some plasma process converts the energy of that beam to radio emission. But the details are critical. What plasma process (that is, which instability) is involved? What conditions are necessary in the plasma for it to happen? Where in the magnetosphere does it go?

These questions can only be answered with a detailed knowledge of the plasma DF. Consider the ongoing discussion about the two-stream instability, and whether or not it can occur in pulsars. The instability goes only if the two plasmas moving relative to each other are “cool”, that is with momentum width less than their separation. In the pulsar context, the two streams are either the electrons and positrons of the pair swarms, or the primary beam moving through the pair swarms. The onset of plasma turbulence

is governed by the temperature and relative motion of the different plasma species (*e.g.*, Weatherall 1994; Usov, this proceedings.). In other words, we need to know the DF.

But this DF has been unclear; in fact, “theorist’s freedom” has prevailed. Some calculations of plasma wave-modes and instabilities have assumed analytically convenient forms (such as boxcars, cold plasma, or relativistic Maxwellians in the star’s frame). Other work has attempted to quantify a plausible, but heuristic, DF introduced by Arons (1981). We hope that our simulations of the true DF will be of use to future work in this area.

### 7.2. Magnetospheric Propagation

The radio emission must travel through the pair plasma, between its emission point and its escape from the star. This propagation can involve “shunting” of radiation along  $\mathbf{B}$ , evolution of the polarization state, and dispersive and scattering effects. The details of the transport, and observable signatures, depend critically on the details of the plasma DF. A familiar example is propagation through the ISM, for which the frequency dependence of scattering and propagation are well known. These signatures can easily be derived from the DF for the ISM, that is a cold, ion-electron plasma, with plasma frequency well below the frequency of the observed radiation. A similar calculation for propagation in a relativistically moving, cold pair plasma predicts that dispersion and scattering in that plasma could be distinguished from ISM propagation at high frequencies (Eilek, 2002; also Lyutikov & Parikh, 2000, or Petrova & Lyubarskii, 2000). We are not aware of any such studies that include a warm plasma, which we now know to be the case.

### 7.3. Shielding

Models of the acceleration region usually assume that the pair plasma can adjust itself to maintain the corotation density, and thus reduce the local  $\mathbf{E}$  to zero, as soon as pair formation goes. This is a great help mathematically, as it allows for straightforward analytic solutions in the acceleration region. However, it may not be supported by more careful consideration of the cascade.

Such shielding depends on two things: the multiplicity of the cascade, and the DF of the pair plasma. If the plasma is cold, and if the electrons and positrons are given a large enough relative streaming velocity (such as a local  $\mathbf{E}_\parallel$  would create), number conservation leads to a finite charge density which can satisfy corotation. Shibata *et al.* (1998) go further, and show that steady space-charge-limited flow is possible for a cold plasma only if the pair multiplicity is very high. This is because newly created opposite-sign charges change the field structure of the acceleration region, and too few pairs (too low an  $\mathcal{M}$ ) cannot support a self-consistent  $\mathbf{E}_\parallel$  field. Their numerical examples require much higher  $\mathcal{M}$  values than our simulations



predict. The issue is further complicated by the creation of warm plasma, as in our simulations. Arendt (2002) applied  $\mathbf{E}_{\parallel}$  fields to induce relative streaming in the post-cascade electron and positron distributions. He found that quite low fields will, indeed, produce a net charge density of the opposite sign, which admits the possibility of shielding. However, a somewhat larger  $E$  field will reverse some of the opposite-sign charges, and thus enhance the original density, because of charges leaving the system.

We are therefore not confident that the pair cascade will always adjust to shield the accelerating  $\mathbf{E}_{\parallel}$ . We suspect pair formation will induce more interesting, non-steady behavior in the plasma.

## 8. How might we observe the plasma?

Theories need to be tested by observations. Is there any way in which we can observe the pulsar plasma?

### 8.1. Indirectly: radio emission and propagation

We observe the plasma indirectly *via* its radio emission. In more conventional astrophysics this allows a simple approach – incoherent emission is well understood. The radio power and spectrum allow the type of emission (synchrotron, bremsstrahlung, *etc.*) to be identified, and the physical conditions (such as density or temperature) in the emitting region to be determined.

This is not so easy for pulsars. We do not have a unique model for coherent radio emission, let alone a simple one. The coherent power is likely to be extremely sensitive to detailed conditions in the plasma, so that modest changes in, say, local density or DF will result in large changes in the instantaneous radio power. Furthermore, the detected pulsar signal probably arises from a highly inhomogeneous region, stratified in density and possibly distributed over altitude.

The situation is further complicated by the fact that the radio signal may have traversed an extended region of the plasma before escaping into “space” and thence to our detectors. The effects of propagation through the ISM are reasonably well understood, but this is not the case for propagation effects within the pulsar magnetosphere.

Thus, interpreting observations of radio power or spectrum directly in terms of the conditions in the emitting region is very difficult. We need alternative methods.

### 8.2. Quasi-directly: temporal fluctuations

Anyone who has looked at pulsar radio data knows that the signal is intrinsically variable on many time scales. The variability can be categorized in terms of observables, and arranged in order of variability timescale.

*Nulls, modes and the mean profile.* The pulsar signal varies dramatically from pulse to pulse, in an apparently

random fashion, and yet each star has a meaningful and stable emission profile when averaged over enough rotation periods (tens to hundreds, depending on the star; *e.g.*, Rathnasree & Rankin 1995). In addition, some stars show nulls or mode changes which persist for many rotation periods. Thus a large-scale order clearly exists within the emission region.

*Drifting subpulses.* Some stars show another type of striking long-term order: drifting subpulses. These are easily identifiable features which drift through the mean profile (*e.g.*, Ramachandran *et al.* 2002). In a few cases they are known to be long-lived, lasting tens of rotation periods, and to circulate around the star’s magnetic axis (Deshpande & Rankin 2001). These occur in some but not all stars; we do not know why.

*Microstructure.* Going to smaller timescales, some stars show microstructure, *i.e.*, significant power on  $\delta t \sim 1 - 100 \mu\text{s}$  (*e.g.*, Lange *et al.* 1998). Once again, microstructure does not exist in all stars (Hankins & Fowler 1982, unpublished) and we do not understand why. The associated scale size  $\lesssim 0.3 - 30 \text{ km} \sim .03 - 3R_*$ . We may be seeing plasma dynamics on scales up to the size of the emission region, or we may be seeing a nonsteady pair cascade.

*Nanostructure.* On even smaller time scales, nanostructure has been detected in giant pulses from the Crab pulsar. There is power on  $\delta t \sim 10 - 100 \text{ ns}$ . We do not know whether this occurs in other stars; only the Crab pulsar has been studied at this time resolution. The associated spatial scale is  $\lesssim 3 - 30 \text{ m}$ ; we are “seeing” quite small structures.

### 8.3. Are these temporal or spatial fluctuations?

There has been much discussion of whether the short-term variability is temporal (due to true time changes in the emitting plasma) or spatial (as a narrow emission beam moves across the sight line). We believe it is temporal, and we argue as follows.

Consider the longer timescales. We can follow individual drifting subpulses for many rotation periods. They are surely due to long-lived plasma structures, moving within the polar cap. The fact that we can identify these structures as they move around the radio emission region (Deshpande & Rankin 2001), means that their emission beam cannot be extremely narrow.

Compare this to the shortest timescales known. If the Crab nanostructure were spatial (as tiny features move past our sightline) the emitting plasma would have to be bunched in very narrow columns,  $\lesssim 1 \text{ cm}$  in width, moving at bulk Lorentz factors of  $\sim 10^7$ . This seems unlikely to us, and contradicts the evidence from drifting subpulses. If

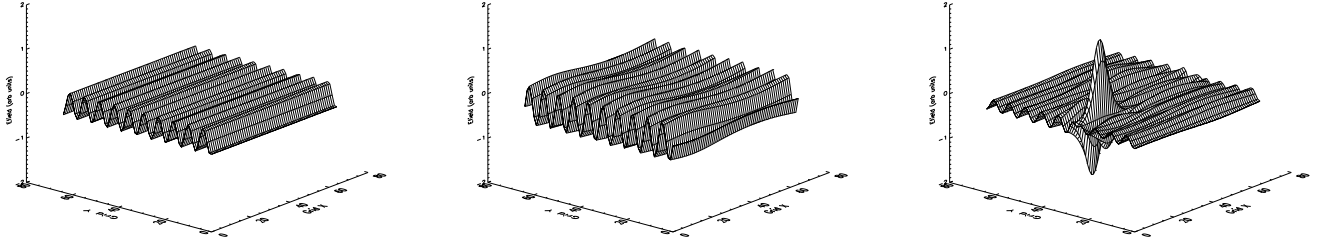


**Fig. 5.** Numerical simulation of the the electric field in strong plasma turbulence. The simulation spans a time interval of  $200/\nu_p$ , and illustrates wave growth by beam-instability (left), modulational instability (center), and wavepacket collapse (right). The extent of the spatial grid is  $64c/\omega_p$ , which scales to to  $60\gamma$  cm at an observing frequency of 5 GHz. The radiation field produced by this collapse is shown in Figure 6. From Weatherall (1997).

microstructure were spatial, the size and Lorentz factors of the required plasma columns would be less extreme, but would still disagree with the subpulse evidence. Based on this, we believe the short-term variability reflects time variability in the emitting plasma.

## 9. Dynamical Variability and Timescales – examples

We know that other plasmas, in the lab and in space, are dynamic and highly variable. We expect the pulsar plasma to be so as well. Thus, our observations of variability in the pulsar signal are indirect observations of the plasma dynamics. With an eye to the general models of the pulsar emission region, described above, we consider time and space scales on which we expect variability.

### 9.1. Micro-scale: the radiating entities

On the smallest space and time scales, the plasma variability will be that which produces coherent radiation. As we noted above, the specific emission process remains a mystery, and several competing models have been suggested. What these models have in common is sensitivity to the microscale dynamics of the underlying plasma. The large-scale structure of the radio-loud region sets the broad stage, but coherent radio emission is generated by evolving plasma structures on much smaller scales. We suspect that each emission process will have a characteristic timescale, which can in principle be observed.

Numerical simulations are needed to follow the plasma evolution and determine the time signature of each model. Weatherall (1997, 1998) has carried out such simulations for the plasma turbulent emission model. In this picture, a two-stream instability drives electrostatic plasma turbulence. When the turbulence becomes nonlinear, the modulation instability produces filamentation of the initial beam-resonant wave, which is followed by “collapse” of the wave along the field direction. Thus, the wave energy accumulates in transient, spatially localized regions. Fig-

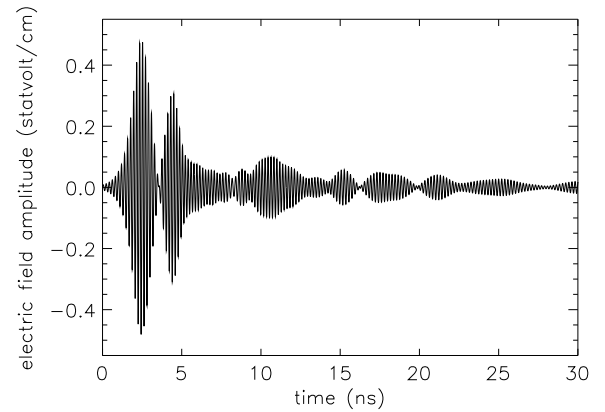


**Fig. 6.** Numerical simulation of a nanopulse: the amplitude of the radiation burst emitted by the strong-turbulence region shown in Figure 5. The characteristic time for radiation emitted at  $\nu_o$  is  $\nu_o\delta t \sim O(10)$ ; this figure has been scaled to an observing frequency of 5 GHz. From Weatherall (1998).

ure 5 shows an example of this growth and collapse. Mode conversion during the explosive collapse phases generates radio emission (the coherence comes from the spatial localization of the plasma oscillation). The simulations reveal a distinctive time signature (Figure 6 shows one example) which comes from the coupling of the radiation modes to the beam-resonant wave. The simulations predict quite narrow band emission,  $\Delta\nu/\nu \sim 0.2$ , centered on the *co-moving* plasma frequency; and predict timescales given by  $\nu\delta t \sim O(10)$  (thus, a few ns at 5 GHz).

Other competing emission mechanisms will have their own characteristic timescales and temporal signatures associated with the “shots”. For instance, curvature emission from coherent plasma bunches might evolve on a particle trapping timescale, *e.g.*,  $(m\lambda/eE)^{1/2}$ , where  $\lambda$  is the bunch length and the field is limited by  $E^2 \lesssim 8\pi\gamma_p mc^2 n_p$ . In addition, the bunch life may be limited by magnetic

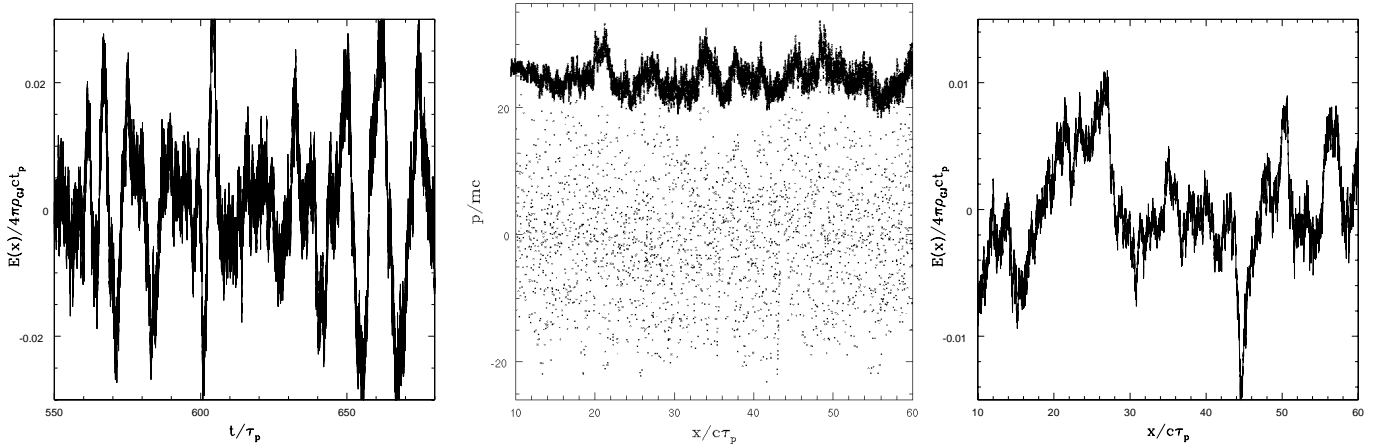


**Fig. 7.** Excitation of strong waves in a sub-GJ current. In this example, which is typical of our numerical experiments, a current density  $j = 0.95j_{\text{GJ}}$  flows from the surface of the star ( $x = 0$  on the grid). The simulation follows the positions and momenta of individual charges, and the electric field evolution in time and space. Left, a partial time series of the  $E$  field at one point of the grid. Center, a phase plot showing the resultant particle trapping. Right, a snapshot of the strong waves in the electric field, at one time during the run. We find that the frequency of the waves excited decreases as  $j/j_{\text{GJ}}$  approaches unity.

field curvature (*e.g.*, Melrose 1992). Combining these, we estimate this process has a longer timescale,  $\sim 0.01 - 0.1\mu\text{s}$ ; but numerical simulations are required to confirm such speculation.

As the emission region is very likely inhomogeneous, containing many microscopic emitting structures (growing and collapsing wave packets, or coherent bunches which grow and dissipate), an observed pulse will be an incoherent collection of such nanobursts. Each nanoburst will contribute an impulse in a shot noise-type model. The individual impulses may be observable if their density is low enough; however a full understanding of the pulse nanostructure requires an understanding of the statistics of such shots. This also requires numerical simulation, and we are extending our plasma-turbulence work to address this issue.

### 9.2. Meso-scale: dynamical fluctuations.

When we consider the intermediate timescales of microstructure, we have likely left the regime of the fundamental radiation process. The associated length scales are comparable to the dimensions of the region (the acceleration region or the radio emission region). Thus, we are “seeing” the dynamical behavior of the radio-loud plasma, as it responds to local forces.

As an example of mesoscale dynamics, consider plasma flow in the acceleration region. The general  $\mathbf{E}$  field in this region, whose divergence is the physical charge density  $\rho$ , can be separated into “corotation” and “other” parts:

$$\tilde{\mathbf{E}} = \mathbf{E} - \mathbf{E}_{\text{co}}; \quad \nabla \cdot \tilde{\mathbf{E}} = 4\pi(\rho - \rho_{\text{GJ}}) \quad (7)$$

The easiest way to follow plasma dynamics in this region is to work in the rotating frame, where the difference field,

$\tilde{\mathbf{E}}$ , controls particle motion. (Compare equation 1, where  $\mathbf{E} = \mathbf{E}_{\text{co}}$  was assumed). Thus, if  $\mathbf{E} \neq \mathbf{E}_{\text{co}}$  (that is if  $\rho \neq \rho_{\text{GJ}}$ ), the plasma feels a net force in the corotating frame.

Now, let the acceleration region sit within a pulsar circuit, so that the local current density is determined by the voltages and resistive loads of the full circuit. This density can easily differ from GJ. If it exceeds GJ (in absolute value), simple space-charge-accelerated flow can occur. If it is somewhat below GJ, however, the situation becomes more complicated. Several authors (*e.g.*, Shibata 1997, or Jessner *et al.*, this proceedings) have noted that steady-flow solutions display strong spatial oscillations when the current is sub-GJ.

We revisit this problem, allowing for time variability. We use a one-dimensional particle-in-cell code to model the space-charge acceleration of plasma escaping from the star’s surface. The simplest situation starts with an external vacuum and a background (corotation) field. For super-GJ flow we verify that the system reaches the steady, space-charge-limited situation,  $\Phi(z) \propto \gamma(z) \propto z^2$  (where  $\Phi$  is the potential and  $z$  is the space coordinate; described *e.g.* by Shibata). In the interesting case of slightly sub-GJ flow, we also find oscillations, but now they are temporal as well as spatial. The outflowing plasma rapidly develops strong waves in the density and  $E$  field, in which feedback and nonlinear growth tends to trap the particles between the wave crests. This trapping slows, but does not stop, the advance of the charge front. A quasi-steady state is reached, in which the current is modulated by strong “trapping” waves. Figure 7 shows an example of this flow. Shibata predicted the spatial wave frequency would depend on the current density; we find this is true also of the temporal frequency. As the current approaches

the corotation value, the oscillations slow down. We have found oscillation periods  $\sim 10 - 100\nu_p^{-1}$  in our simulations to date, which could be observable as microstructure if  $\nu_p$  is identified with the observing frequency.

Our simulations do not include emission of escaping radiation. Thus, we cannot directly predict the time signature of the coherent radiation emitted by this plasma. That radiation will arise through the interaction of plasma charges and waves riding within the meso-scale structure which these simulations describe. We anticipate, however, that the density and field modulations seen in this non-stable system will be echoed in the escaping radiation. Thus, pulsars with strong microstructure signatures may be ones in which the current is close to but below the corotation current.

We expect similar results in other situations. One example is pair formation, which might disrupt an initially steady flow. Laboratory diodes are difficult to maintain in a steady state, because plasma formation at the diode disrupts the current, leading to strong waves and breakdown of the steady flow. We expect that pair formation in a pulsar acceleration region will have a similar effect. Rapid injection of new plasma in a steady-flow region will disrupt the flow, leading to temporal variability that may be observable.

### 9.3. Macro-scale: self organization.

On longer timescales, many rotation periods, we leave plasma microphysics and go to larger-scale, MHD effects. These timescales are the most accessible observationally, and perhaps the most daunting theoretically.

One striking example is the long-lived drifting subpulses seen in some stars. Their drift rate is consistent with the  $\mathbf{E} \times \mathbf{B}$  drift due to the non-corotation  $\mathbf{E}$  field predicted by well-known models of the acceleration region (*e.g.*, Ruderman & Sutherland, 1975, or Arons & Scharlemann, 1978). The mystery of the drifting subpulses is their stability; the analysis of Deshpande & Rankin (2000) suggests that individual radio-loud structures retain their identity for 10–100 rotation periods. They have been modelled as “sparks” of localized pair creation, which may partially shield their immediate surroundings (*e.g.*, Ruderman & Sutherland). This does not seem to be the entire picture, however. Why should such sparks be so long-lived?

It is tempting to speculate that these long-lived plasma filaments are the result of a saturated plasma instability. Such features – for instance, quasi-stable, current-aligned filaments – are common in other plasma environments. The problem is how to make them. The radio-loud pulsar plasma is very highly magnetized, as shown by the energy ratio

$$\beta = \frac{8\pi\gamma n m c^2}{B^2} \sim 1 \times 10^{-18} \frac{\gamma n}{n_{\text{GJ}}} \left(\frac{r}{r_*}\right)^3 \quad (8)$$

(we have scaled the number density to the corotation value, the  $B$  field to its value at the star’s surface, and assumed a dipole field). This shows that one must go to quite high altitudes before the plasma inertia becomes comparable to the magnetic energy density (so that normal MHD instabilities might be expected). Resistive instabilities are tempting; they are known to occur in low- $\beta$  plasmas and can lead to field-aligned filaments. We agree with Melrose (2000) who suggested such structures in the context of the density problem. It may be that filaments exist in all pulsars at some level, and happen to be stronger or longer-lived in those with clear subpulse drift. However, without a good understanding of such details as cross-field resistivity in this environment, we can do no more than speculate on this interesting question.

## 10. A Case Study: Giant Pulses in the Crab pulsar

The Crab pulsar emits occasional “giant” pulses which can be thousands of times more intense than an average pulse. One of us (Hankins, with his colleagues) is making ultra-high time resolution observations of these giant pulses. The data can give us insight into the emission mechanism and the dynamics of the emitting plasma. In this section we present preliminary results which bear on the physics of the emission region.

### 10.1. Observations and Pulse Structure

Using the VLA in phased-array mode minimizes the signal from the surrounding nebula, and allows us to study individual giant pulses at time resolution down to a few ns. To achieve this we used coherent dedispersion. The incoming voltage is Nyquist sampled at 100 MHz. The samples are recorded for later, off-line processing which removes dispersion distortion. The signals are passed through a filter whose transfer function is the inverse of the (frequency-dependent) phase change imposed by propagation through the ISM. This technique allows us to recover the full time resolution of the emitted signal, limited only by the receiver bandwidth.

We reached 10 ns resolution at several frequencies from 1.4 to 15 GHz, making single frequency observations and also doing simultaneous observations at two frequencies. Individual pulses are quite complex when seen at this resolution. They often contain clear subpulses, which usually have a “Fred” shape (“Fast Rise, Exponential Decay”). Figures 8 - 11 show some examples. The subpulse widths are typically  $\sim 1\mu\text{s}$  at 5 GHz, and  $\sim 0.1\mu\text{s}$  at 8 GHz. (We note that unresolved features can be found down to our resolution limit of 10 ns.)

Above  $\sim 2$  GHz we clearly see the intrinsic pulse shape; below  $\sim 1$  GHz the pulse width is dominated by nebular or interstellar scattering (ISS). In the range  $\sim 1 - 2$  GHz single pulses or subpulses show the “Fred” shape charac-

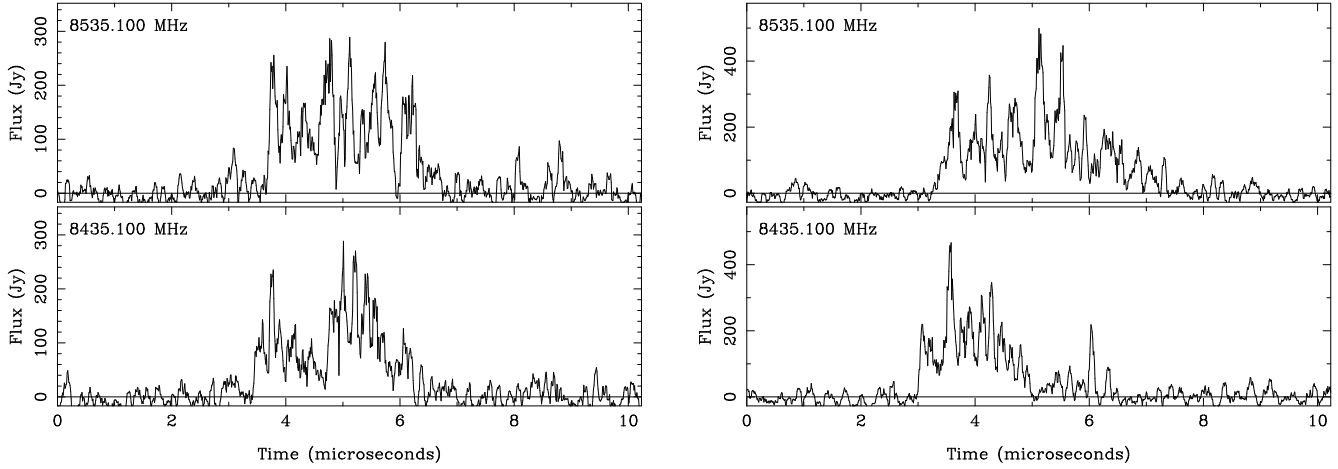


**Fig. 8.** Two single giant pulses from the interpulse of the Crab pulsar, each recorded simultaneously at 8.4 and 8.5 GHz. The data were obtained (after coherent dedispersion; §10.1) at 10 ns time resolution, and have been block smoothed to 80 ns. The dispersion delay has been removed.

teristic of scattering, but have widths which do not follow the  $\nu^{-4}$  law expected for ISS, and are strongly variable on a timescales less than an hour (too short to be from variations in the ISM). The average pulse width at high frequencies decays only slowly with frequency, and may obey  $\Delta t(\nu) \propto \nu^{-2}$  (Moffett, 1997). We suspect that propagation through the magnetosphere broadens high-frequency subpulses and give them the “Fred” shape. Turbulent scattering in a cold, relativistically streaming pair plasma in fact gives the observed frequency signature (Eilek, 2002).

### 10.2. Emission bandwidth

Giant pulses in the Crab pulsar occur simultaneously over a broad frequency range, at least from 1.4 to 4.8 GHz. Thus, in some sense the emission is broad-band.

However, the situation becomes more complex if we consider substructure within a giant pulse. Our simultaneous two-frequency data suggest that the intrinsic emission bandwidth of *substructure* is narrow band. Compare Figures 8-10 in which we present simultaneous dual-frequency measurements of individual giant pulses. While we have not yet completed a statistical analysis of our two-frequency observations, our impression after working with the data is that the substructure in a giant pulse is well correlated if the two frequencies are close: 1.4 and 1.7 GHz, 4.5 and 5.0 GHz, or 8.4 and 8.5 GHz. However, the substructure is less well correlated over a broader frequency range, such as 1.4 and 4.8 GHz. This suggests that the bandwidth of a given *subpulse* obeys  $0.2 \lesssim \Delta\nu/\nu < 1$ . Comparing this to the simulations by Weatherall (1998), we note that the observations are consistent with what his model predicts.

### 10.3. Energy content

Another interesting hint in the data is that individual subpulses conserve total energy,  $E = \int I(t)dt$ . We have fitted several data sets at 1.4, 4.8 and 8.4 GHz with the “Fred”-like function  $I(t) = I_0 te^{-t/\tau}$ , allowing multiple subpulses per giant pulse. Figure 11 shows examples of such fits. Typical results are shown in Figure 12. A plot of intensity  $I_0$  against width  $\tau$  shows an upper envelope, which is consistent with  $E \propto I_0\tau = \text{constant}$ . This is what one would expect if each subpulse results from a “collect and release” process, in which internal energy is stored until a threshold is reached, then suddenly released. The constant-energy envelope of the distribution then describes the total energy released in the burst, and the points below the envelope are what we would expect if the released energy is relativistically beamed at some angle to the line of sight.

We caution the reader that these results are preliminary, and require a careful statistical analysis of a larger, complete sample of high-frequency subpulses (currently underway). If further work supports our speculation, that the subpulses in giant pulses have an upper limit to their energy content, then the difference between this conclusion and the energy distribution of giant pulses presented by Lundgren *et al.* (1995) must be addressed. We note two differences between our work and theirs. We are considering subpulses, several of which may be contained in a giant pulse. In addition, our higher time resolution allows us to separate subpulse width and height, which may make the upper energy limit more apparent.

### 10.4. The emission region in the Crab pulsar

From these data, we begin to draw a picture of the radio-loud plasma in the Crab pulsar. It is inhomogeneous and fluctuates on quite short timescales. Any given piece of the plasma is a narrow-band radio emitter; the larger fre-

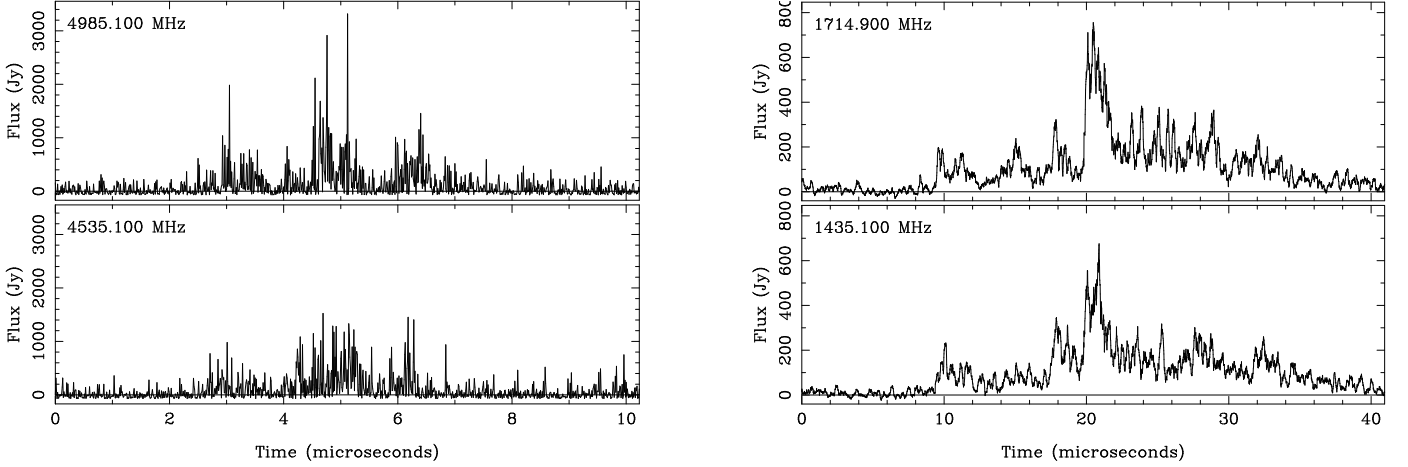


**Fig. 9.** Two single giant pulses from the Crab pulsar. Left, a pulse recorded simultaneously at two frequencies within C band, with time resolution 10 ns. Right, a (different) pulse recorded simultaneously at two frequencies within L band; the data have been smoothed to 200 ns. The dispersion delay has been removed for each pulse. These pulses illustrate the typical behavior of the star. The subpulses and micro-bursts are similar but not identical. Such data suggest that the intrinsic bandwidth of an individual “burst” of emission is at least  $\delta\nu/\nu \sim 0.2$ .

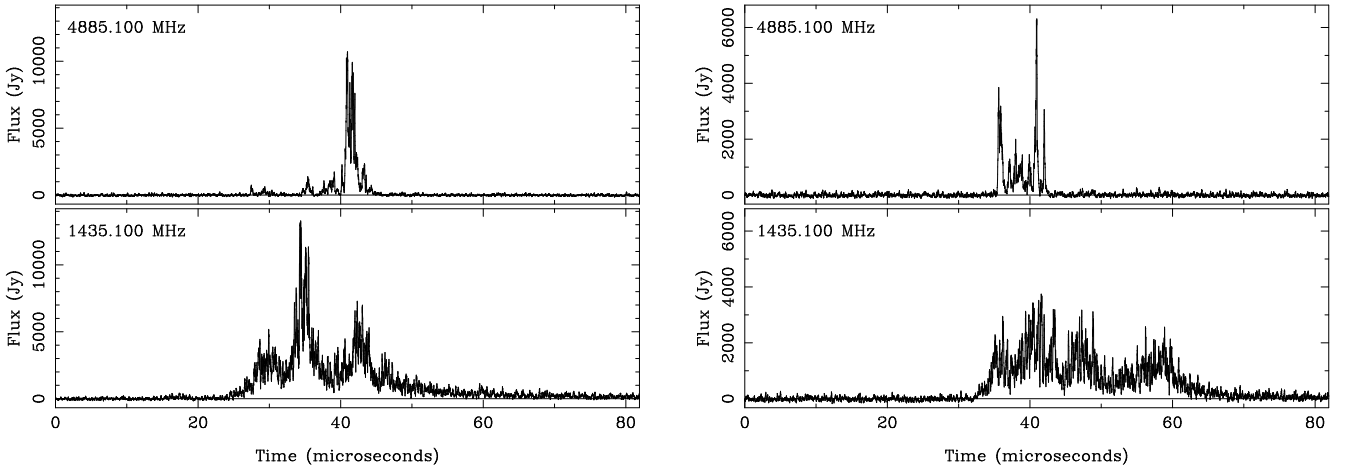


**Fig. 10.** Two more single giant pulses from the Crab pulsar. Each was recorded simultaneously at 5 and 1.4 GHz, obtained at 10 ns time resolution and smoothed to 100 ns. The dispersion delay has been removed. These two pulses are not as well correlated, over this larger frequency separation, as are the two illustrated in Figure 9. This behavior is typical of the star. We infer that the emission bandwidth of the microbursts which constitute an individual “giant pulse” is narrower than this frequency separation. Comparing this with data such as in Figure 9, we infer the intrinsic emission bandwidth obeys  $0.2 \lesssim \Delta\nu/\nu < 1$ , and that a giant pulse contains a collection of many such microbursts, distributed over a range of central emission frequencies.

quency range of an individual giant pulse probably comes from the variable density within the region. A giant pulse seems to trace the simultaneous excitation of an extended region of plasma, in which different sub-regions independently reach some critical threshold and then release their stored energy in sudden, observable bursts.

**Acknowledgements.** We have learned a great deal about pulsar physics through discussion with a number of people, including Jon Arons, Gregory Benford, Janusz Gil, Wolfgang Kundt, Harald Lesch, Leon Mestel, Don Mel-

rose and Dipanjan Mitra. We particularly appreciate the enthusiasm and hard questions supplied by Jeff Kern and Axel Jessner, and we thank Axel for his careful reading of this long paper. Work by the Socorro pulsar group has been partially supported by NSF grants AST-9315285 and AST-9618408. JE appreciates support and hospitality from the Heraeus foundation and the MPIfR while this paper was being written.

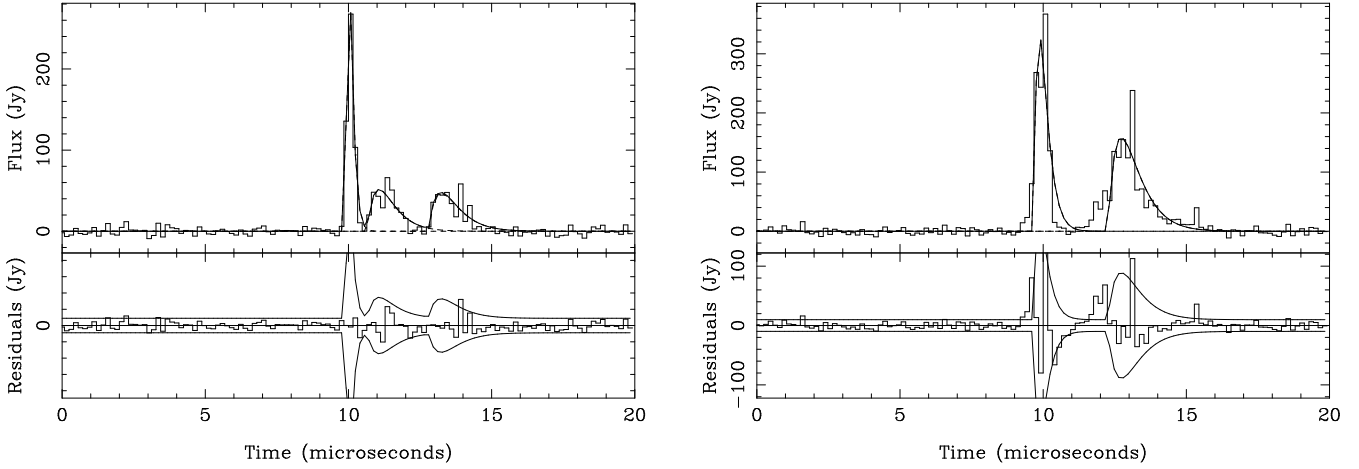


**Fig. 11.** Two representative X band pulses, illustrating “Fred” fits to subpulses. The data were fitted with a function  $I(t) \propto I_o t e^{-t/\tau}$ . (Thus,  $I_o$  measures the pulse height,  $\tau$  the width, and the total energy  $\propto I_o \tau$ .) The upper plot shows the original data, taken at 8415 MHz and smoothed to 160 ns resolution, and the result of the “Fred” fits. The lower plot shows the  $2\sigma$  estimation error of the fit and the fit residuals. The intensity  $I_o$  and width  $\tau$  for a set of these fits are plotted in Figure 12.

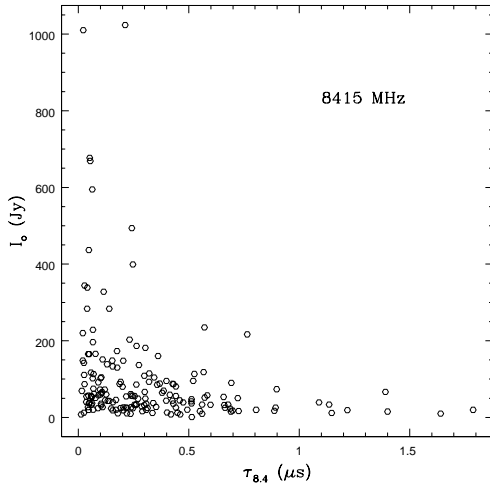


**Fig. 12.** Intensity *vs.* width for subpulse fits for one data set. The plot shows  $(\tau, I_o)$  from fits to 180 subpulses identified in a set of 60 giant pulses, recorded within a bit over an hour at 8.4 GHz at the VLA. There is a tendency for weak pulses to be broad and strong pulses to be narrow; a constant energy ( $I_o \propto 1/\tau$ ) envelope seems to exist.

## References

- Arendt, P. N. Jr, 2002, Ph.D. thesis, New Mexico Tech  
Arendt, P. N. Jr. & Eilek, J. A., 2002, submitted to ApJ.  
Arons, J., 1981, in Proc. Varenna Summer School on Plasma Astrophysics, ed. T. D. Guyenne & G. Lévy (Noordwijk: ESA), 273  
Arons, J. & Scharlemann, E. T., 1979, ApJ, 231, 854  
Asseo, E., Pelletier, G. & Sol, H., 1990, MNRAS, 247, 529  
Eilek, J. A., 2002, submitted to ApJ  
Eilek, J. A. & Hankins, T. H., 2000, in IAU Colloquium 177, Pulsar Astronomy–2000 and Beyond, eds., M. Kramer, N. Wex & R. Wielebinski (San Francisco: ASP), 721  
Eilek, J. A. & Hankins, T. H., 2002, in preparation  
Daughtery, J. K. & Harding, A. K., 1982, ApJ, 252, 337  
Deshpande, A. A. & Rankin, J. M., 2001, MNRAS, 322, 438  
Hankins, T. H. & Rankin, J. R., 2002, in preparation.  
Hibschman, J. A. & Arons, J., 2001, ApJ, 560, 871  
Jessner, A., Lesch, H. & Kunzl, T., 2001, ApJ, 547, 959  
Kazbegi, A. Z., Machabeli, G. Z. & Melikidze, G. I., 1995, MNRAS, 253, 377  
Kijak, J. & Gil, J., 1997, MNRAS, 288, 631  
Kunzl, T., Lesch, H., Jessner, A. & von Hoensbroech, A., 1998, ApJ, 505, L139  
Kunzl, T., Lesch, H. & Jessner, A., 2002, submitted to A&A  
Lange, C., Kramer, M., Wielebinski, R. & Jessner, A., 1998, A&A, 332, 111  
Lundgren, S. C., Cordes, J. M., Ulmer, M., Matz, S. M., Lomatch, S., Foster, R. S. & Hankins, T. H., 1995, ApJ, 453, 433  
Luo, Q. & Melrose, D. B., 1995, MNRAS 276, 372  
Lyutikov, M. & Parikh, A., 2000, ApJ, 541, 1016.  
Melrose, D. B., 1992, in IAU Colloquium 128, ed. T. H. Hankins, J. M. Rankin & J. A. Gil (Zielona G'ora: Pedagogical Univ. Press), 307  
Melrose, D. B., 2000, in IAU Colloquium 177, eds., M. Kramer, N. Wex & R. Wielebinski (San Francisco: ASP), 721  
Moffett, D., 1997, Ph.D. thesis, New Mexico Tech  
Petrova, S. A. & Lyubarskii, Y. E., 2000, A&A, 355, 1168  
Ramachandran, R., Rankin, J. M., Stappers, B.W., Kouwenhoven, M.L. A., & van Leeuwen, A. G. J., 2002, submitted to A&A  
Rankin, J. R., 1993, ApJ, 405, 285  
Rathnasree, N. & Rankin, J. R., 1995, ApJ, 452, 814  
Ruderman, M. A. & Sutherland, P. G., 1975, ApJ, 196, 51  
Shibata, S., 1991, ApJ, 278, 239  
Shibata, S., 1997, MNRAS 287, 262

- Shibata, S., Miyazaki, J. & Takahara, F., 1998, MNRAS 295,  
L53
- Sturmer, S., 1995, ApJ, 446, 292
- van Hoensbroech, A. & Xilouris, K. M., 1997, A&A, 126, 121
- Weatherall, J. C., 1994, ApJ, 428, 261
- Weatherall, J. C., 1997, ApJ, 483, 402
- Weatherall, J. C., 1998, ApJ, 506, 341
- Weatherall, J. C., 2001, ApJ, 559, 196
- Weatherall, J. C. & Eilek, J. A., 1997, ApJ, 474, 407